

# Proton $G_E/G_M$ from beam-target asymmetry

M. K. Jones,<sup>1</sup> A. Aghalaryan,<sup>2</sup> A. Ahmidouch,<sup>3</sup> R. Asaturyan,<sup>2</sup> F. Bloch,<sup>4</sup> W. Boeglin,<sup>5</sup> P. Bosted,<sup>1</sup> C. Carasco,<sup>4</sup> R. Carlini,<sup>1</sup> J. Cha,<sup>6</sup> J.P. Chen,<sup>1</sup> M.E. Christy,<sup>7</sup> L. Cole,<sup>7</sup> L. Coman,<sup>5</sup> D. Crabb,<sup>8</sup> S. Danagoulian,<sup>3</sup> D. Day,<sup>8</sup> J. Dunne,<sup>6</sup> M. Elaasar,<sup>9</sup> R. Ent,<sup>1</sup> H. Fenker,<sup>1</sup> E. Frlez,<sup>8</sup> D. Gaskell,<sup>1</sup> L. Gan,<sup>10</sup> J. Gomez,<sup>1</sup> B. Hu,<sup>7</sup> J. Jourdan,<sup>4</sup> C. Keith,<sup>1</sup> C.E. Keppel,<sup>7</sup> M. Khandaker,<sup>11</sup> A. Klein,<sup>12</sup> L. Kramer,<sup>5</sup> Y. Liang,<sup>7</sup> J. Lichtenstadt,<sup>13</sup> R. Lindgren,<sup>8</sup> D. Mack,<sup>1</sup> P. McKee,<sup>8</sup> D. McNulty,<sup>8</sup> D. Meekins,<sup>1</sup> H. Mkrtchyan,<sup>2</sup> R. Nasseripour,<sup>5</sup> I. Niculescu,<sup>1</sup> K. Normand,<sup>4</sup> B. Norum,<sup>8</sup> D. Pocanic,<sup>8</sup> Y. Prok,<sup>8</sup> B. Raue,<sup>5</sup> J. Reinhold,<sup>5</sup> J. Roche,<sup>1</sup> D. Rohe,<sup>4</sup> O.A. Rondón,<sup>8</sup> N. Savvinov,<sup>14</sup> B. Sawatzky,<sup>8</sup> M. Seely,<sup>1</sup> I. Sick,<sup>4</sup> K. Slifer,<sup>8</sup> C. Smith,<sup>8</sup> G. Smith,<sup>1</sup> S. Stepanyan,<sup>2</sup> L. Tang,<sup>7</sup> S. Tajima,<sup>8</sup> G. Testa,<sup>4</sup> W. Vulcan,<sup>1</sup> K. Wang,<sup>8</sup> G. Warren,<sup>4,1</sup> F.R. Wesselmann,<sup>8,11</sup> S. Wood,<sup>1</sup> C. Yan,<sup>1</sup> L. Yuan,<sup>7</sup> J. Yun,<sup>15</sup> M. Zeier,<sup>8</sup> and H. Zhu<sup>8</sup>

(The Resonance Spin Structure Collaboration)

<sup>1</sup>Thomas Jefferson National Accelerator Facility, Newport News, Virginia 23606

<sup>2</sup>Yerevan Physics Institute, Yerevan, Armenia

<sup>3</sup>North Carolina A&T State University, Greensboro, North Carolina 27411

<sup>4</sup>Universität Basel, CH-4056 Basel, Switzerland

<sup>5</sup>Florida International University, Miami, Florida 33199

<sup>6</sup>Mississippi State University, Mississippi State, Mississippi 39762

<sup>7</sup>Hampton University, Hampton, Virginia 23668

<sup>8</sup>University of Virginia, Charlottesville, Virginia 22903

<sup>9</sup>Southern University at New Orleans, New Orleans, Louisiana 70126

<sup>10</sup>University of North Carolina, Wilmington, North Carolina 28403

<sup>11</sup>Norfolk State University, Norfolk, Virginia 23504

<sup>12</sup>Old Dominion University, Norfolk, Virginia 23529

<sup>13</sup>Tel Aviv University, Tel Aviv, 69978 Israel

<sup>14</sup>University of Maryland, College Park, Maryland 20742

<sup>15</sup>Virginia Polytechnic Institute & State University, Blacksburg, Virginia 24061

(Dated: September 3, 2018)

The ratio of the proton's electric to magnetic form factor,  $G_E/G_M$ , can be extracted in elastic electron-proton scattering by measuring either cross sections, beam-target asymmetry or recoil polarization. Separate determinations of  $G_E/G_M$  by cross sections and recoil polarization observables disagree for  $Q^2 > 1$  (GeV/c)<sup>2</sup>. Measurement by a third technique might uncover an unknown systematic error in either of the previous measurements. The beam-target asymmetry has been measured for elastic electron-proton scattering at  $Q^2 = 1.51$  (GeV/c)<sup>2</sup> for target spin orientation aligned perpendicular to the beam momentum direction. This is the largest  $Q^2$  at which  $G_E/G_M$  has been determined by a beam-target asymmetry experiment. The result,  $\mu G_E/G_M = 0.884 \pm 0.027 \pm 0.029$ , is compared to previous world data.

PACS numbers: 25.30.Bf, 13.40.Gp

## I. INTRODUCTION

Understanding the structure of the nucleon has long been a goal of nuclear physics and elastic electron-nucleon scattering has been an important tool in this quest. In the one-photon exchange (Born) approximation, the structure of the nucleon can be characterized in terms of the electric and magnetic form factors,  $G_E$  and  $G_M$ , which depend only on the four-momentum transfer squared,  $Q^2 = -t$ . At  $Q^2 = 0$ , the proton form factors are defined as  $G_E = 1$  and  $G_M = \mu$ , where  $\mu = 2.7928$  is the proton's magnetic moment. The proton form factors can be extracted individually in elastic electron-proton scattering by measuring cross sections at the same  $Q^2$  but different beam energies (Rosenbluth technique). In addition, spin observables in elastic electron-proton scattering are sensitive to the ratio of  $G_E$  to  $G_M$ .

Historically, the Rosenbluth technique was used to

measure  $G_E$  and  $G_M$  with elastic scattering identified by detection of the scattered electron. The cross section can be written as:

$$\begin{aligned} \frac{d\sigma}{d\Omega} &= \frac{\alpha^2 E' \cos^2 \frac{\theta_e}{2}}{4(1+\tau)E^3 \sin^4 \frac{\theta_e}{2}} \left[ G_E^2 + \frac{\tau}{\epsilon} G_M^2 \right] \quad (1) \\ \tau &= \frac{Q^2}{4M^2} \quad Q^2 = 2EE'(1 - \cos \theta_e) \\ \epsilon &= \left[ 1 + 2(1+\tau) \tan^2 \frac{\theta_e}{2} \right]^{-1} \end{aligned}$$

where  $E$  and  $E'$  are the incoming and outgoing electron energies,  $M$  is the proton mass and  $\theta_e$  is the outgoing electron's scattering angle.  $G_M$  in Eq. 1 is multiplied by  $Q^2$  and dominates the cross sections at large  $Q^2$  at all  $\epsilon$ . For example, at  $Q^2 = 6$  (GeV/c)<sup>2</sup>, the contribution of  $G_E$  to the elastic cross section is 7% at  $\epsilon = 0.9$ , assuming  $\mu G_E/G_M = 1$ .

At SLAC,  $G_E/G_M$  was measured to  $Q^2 = 8.8$  (GeV/c)<sup>2</sup> using the Rosenbluth technique [1]. A recent JLab Hall C experiment [2] in the same  $Q^2$  range agrees with the SLAC data. These data were combined together with other cross sections measurements for a global analysis by Arrington [3]. The  $\mu G_E/G_M$  extracted from the global analysis is plotted in Fig. 1 and labeled “World xn”. The dashed line in Fig. 1 is  $\mu G_E/G_M$  from a fit by Arrington to that data with a polynomial parametrization of  $G_E$  and  $G_M$ .

Previous cross sections measurements detected electrons to identify an elastic event. A recent JLab experiment [4] in Hall A identified an elastic scattering event by detection of the scattered proton. This experimental approach has different systematic errors compared to electron detection and has many advantages in terms of reducing the systematic error. The  $\mu G_E/G_M$  are plotted in Fig. 1 and labeled as “JLAB05”. The new data agree well with the recent fit to previous world data which demonstrates that the systematic errors in the Rosenbluth technique are understood.

Early on, it was proposed [5, 6, 7] that measuring polarization observables in elastic electron-proton scattering would be an alternative method to extract the electric form factor given that the dominant magnetic form factor is determined by cross section data. In 1976, an experiment [8] measured the beam-target asymmetry for elastic  $ep$  scattering at  $Q^2 = 0.76$  (GeV/c)<sup>2</sup>. But given that the experiment used a longitudinally polarized target, the asymmetry was extremely insensitive to  $G_E/G_M$  and could only restrict the relative sign between  $G_E$  and  $G_M$ .

With the advent of high duty factor, high current, and highly polarized electron beam accelerators such as Jefferson Lab and the Mainz Microtron, experiments which measure the proton and neutron electro-magnetic form factors have reached a new level of precision over a larger  $Q^2$  range by measuring polarization observables in elastic electron-nucleon scattering (see Ref. [9] for a review of the recent experiments). The proton  $G_E/G_M$  ratios have been extracted from measurement of the recoil polarization components of the scattered protons in elastic scattering of polarized electrons from an unpolarized proton target. Both the transverse,  $P_x$ , and longitudinal,  $P_z$ , components of scattered proton’s recoil polarization are dependent on  $G_E/G_M$ . By simultaneously measuring both components, one can extract  $G_E/G_M$  from the ratio of polarization components,  $P_x/P_z$ , which cancels systematic errors from the beam polarization and the analyzing power.

The first measurements of  $G_E/G_M$  using the polarization transfer technique were done at MIT-Bates [10] in the 1990’s at  $Q^2 = 0.38$  and  $0.5$  (GeV/c)<sup>2</sup> and are plotted in Fig. 1. The results agree with  $G_E/G_M$  from the Rosenbluth technique. The polarization transfer technique was used in Hall A at Jefferson Lab [11, 12] to measure  $G_E/G_M$  to  $Q^2 = 5.6$  (GeV/c)<sup>2</sup> and the data are plotted in Fig. 1. A linear fall-off with  $Q^2$  is seen

which is in sharp contrast to the nearly flat  $Q^2$  dependence of  $G_E/G_M$  measured with the Rosenbluth technique. The absolute systematic error on the polarization transfer technique is given by the solid band at the bottom of Fig. 1. Reconciling the  $G_E/G_M$  results from the two techniques is impossible given the systematic error quoted for both techniques. A recent result [13] using the polarization transfer technique in Hall C at Jefferson Lab for  $G_E/G_M$  at  $Q^2 = 1.13$  (GeV/c)<sup>2</sup> is plotted in Fig. 1 with the error bar that is dominated by statistics.

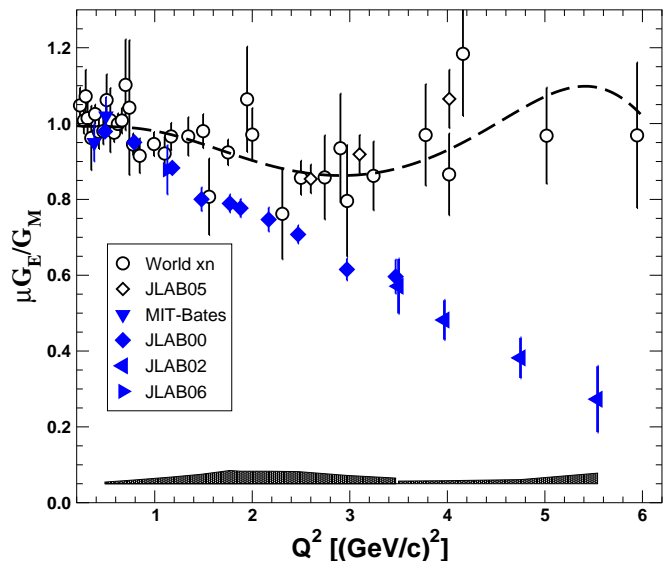


FIG. 1: (Color online) Ratio  $\mu G_E/G_M$  plotted as a function of  $Q^2$ . “World xn” and JLAB05 [4] used the Rosenbluth technique. Results using the recoil polarization technique are from MIT-Bates [10], JLAB00 [11], JLAB02 [12] and JLAB06 [13]. The band at the bottom is the systematic error on the data from JLAB00 and JLAB02. The dashed curve is a recent fit [3] to the world cross section data.

One possible solution that reconciles the different  $G_E/G_M$  from the two experimental techniques is inclusion of two-photon exchange mechanisms which are not part of the standard radiative correction procedure which reduces the raw cross section data to the Born cross sections needed in Eq. 1 for determination of  $G_E$  and  $G_M$ . The Coulomb distortion effect is one type of two-photon exchange mechanism (exchange of one hard and one soft photon) which has been neglected in  $ep$  experiments. Calculations [14] which include Coulomb distortion effects when extracting the form factors from the cross sections find that  $\mu G_E/G_M$  is reduced by about 0.05 for  $Q^2 > 1$  (GeV/c)<sup>2</sup> while the effect on  $\mu G_E/G_M$  is gradually reduced at smaller  $Q^2$ .

More general calculations [15, 16] of the contribution of two-photon exchange mechanisms in elastic electron-proton scattering have been done. The two calculations take different approaches to the model of the nucleon which is needed as part of the two-photon exchange calculation. The approach of Ref. [15] is applicable to lower

$Q^2$  then that of Ref. [16]. In both calculations, the contribution of the two-photon exchange amplitude has an  $\epsilon$ -dependence which has the same sign as the  $G_E$  contribution to the cross section and is large enough to effect the extracted value of  $G_E$ . Therefore, the extracted  $G_E/G_M$  for the Rosenbluth technique is reduced.

In addition to a linear  $\epsilon$ -dependence, both calculations have a nonlinear  $\epsilon$ -dependence in the two-photon contribution to the cross section. A global analysis [17] of the  $\epsilon$ -dependence of elastic and inelastic cross sections found that the elastic (inelastic) data was consistent with a maximum deviation from a linear fit of  $\leq 0.4\%$  ( $0.7\%$ ). But this level of precision is obtained by averaging over  $0.2 < Q^2 < 5.2$   $(\text{GeV}/c)^2$  range. Since the amount of nonlinearity can change with  $Q^2$ , more precise data is needed for comparison to theory. An approved JLab experiment [22] is an extensive study of non-linearity in the  $\epsilon$ -dependence of the elastic electron-proton cross section at fixed  $Q^2$  for a number of different  $Q^2$ .

The effect of two-photon exchange amplitude on the polarization components is small, though the size of the contribution changes with  $\epsilon$ . The recoil polarization measurements at JLab ran at  $\epsilon$  between 0.45 and 0.77. From Ref. [15], the measured  $P_x/P_z$  at  $\epsilon = 0.5$  should be reduced by factors of 0.9975 and 0.97 at  $Q^2 = 1$  and 6  $(\text{GeV}/c)^2$ , respectively. At  $Q^2 = 3$   $(\text{GeV}/c)^2$ , Ref. [15] predicts that  $P_x/P_z$  will be 4% larger at  $\epsilon = 0.05$  compared to  $\epsilon = 1$  due to contributions from two-photon amplitudes. Interestingly, the calculation of Ref. [16] predicts that  $\epsilon$ -dependence of  $P_x/P_z$  will have a slope of the opposite sign. Complementing the approved JLab cross section experiment, an upcoming JLab experiment [18] will measure the  $\epsilon$ -dependence of  $P_x/P_z$  at  $Q^2 = 2.6$   $(\text{GeV}/c)^2$ .

The two-photon models need to be tested by comparing predictions of additional observables to data. Experiments planned at Jefferson Lab [19] and proposed at VEPP-3 in Novosibirsk [21] would precisely measure the  $\epsilon$ -dependence of the ratio of cross sections,  $R_{e+e-}$ , for elastic electron-proton scattering to positron-proton scattering at a fixed  $Q^2$ . In absence of two-photon mechanisms, the ratio would be one and independent of beam energy. The present data set for  $R_{e+e-}$  is limited with most measurements at  $\epsilon > 0.6$ . Previous experimental data was re-examined [20] and found that combining all data for  $Q^2 < 2$   $(\text{GeV}/c)^2$  gives a slope of  $-5.7 \pm 1.8$  % for the  $\epsilon$ -dependence of  $R_{e+e-}$ . Indeed, the calculation of Ref. [15] predicts an  $\epsilon$ -dependence which is consistent with the large error bars of the existing data.

Checking on the possibility of an unknown systematic error in the Rosenbluth or recoil polarization technique is also important. Measurement of the beam-target asymmetry in elastic electron-proton scattering offers an independent technique of determining  $G_E/G_M$ . The systematic errors are different when compared to either the Rosenbluth technique or the polarization transfer technique. For elastic scattering, the recoil polarization of scattered proton is directly related to the beam-target

asymmetry by time reversal invariance. Therefore, sensitivity of the beam-target asymmetry to two-photon effects is the same as in the recoil polarization technique. By measuring  $G_E/G_M$  by a third technique and comparing to previous results, the discovery of unknown or underestimated systematic errors in the previous measurements is possible.

## II. EXPERIMENTAL SET-UP

The experiment was performed in Hall C at the Thomas Jefferson National Accelerator Facility (Jefferson Lab). The main purpose of the experiment was a measurement of the inclusive parallel and perpendicular spin asymmetries in the resonance region for electron scattering on polarized proton and deuterium targets. This report presents a subset of the data which measured the perpendicular beam-target asymmetry for elastic electron-proton scattering.

Polarized electrons with 5.755 GeV/c momentum were scattered from polarized frozen ammonia ( $^{15}\text{NH}_3$ ) with the spin of the polarized target aligned perpendicular to the beam. The scattered electrons were detected at  $13.15^\circ$  in the High Momentum Spectrometer (HMS) which was set at a central momentum of 4.73 GeV/c. Electron particle identification was done by a combination of a gas Cerenkov detector and lead-glass calorimeter. A cut was placed to use a momentum range of  $\pm 8\%$ .

The frozen ammonia target [23] is polarized by dynamic nuclear polarization and operated at 1 K in a 5 T magnetic field. The magnetic field is created by a pair of superconducting Helmholtz coils which produces a uniform magnetic field that selects the spin direction of the protons. The refrigerator is a  $^4\text{He}$  evaporation type which is installed vertically along the center of the magnet. The coils can be rotated independently of the refrigerator so that the target spin can be aligned to any angle relative to the beam. The angle of the coils relative to the beam was measured to a precision of  $0.1^\circ$ .

To make the target, frozen ammonia is pulverized into small fragments which are sifted to get fragments of the same size. The fragments are stored in sample bottles in liquid nitrogen dewars. For use in the experiment, the ammonia fragments are placed in a cylindrical container which is 3 cm long with a diameter of 2.5 cm. Inside the container is a coil for measuring the NMR signal. The container is placed on an insert ladder so that the beam passes through the container lengthwise. The insert ladder can be rotated independently of the magnet coils and refrigerator so that the beam enters the container perpendicular to its face. To check the orientation of the insert ladder, a target was placed on the insert which consisted of L-shaped rods of tungsten separated by 3cm. From reconstruction of the rods, the insert ladder was determined to be rotated  $6^\circ$  relative to the beam direction. The insert ladder held two frozen ammonia containers which were designated as TOP and BOTTOM. Addi-

tional targets on the insert were a 6.9-mm-thick  $^{12}\text{C}$  disk and an empty container. The targets are in a bath of liquid helium that is cooled by the refrigerator.

To maintain reasonable target polarization, the beam current was limited to 100 nA and was uniformly rastered. The uniformity of the raster was obtained by independently and simultaneously rastering at a fast frequency (17.9 kHz in vertical direction and 24.2 kHz in the horizontal direction) over 1 mm square spot and slow frequency (30 Hz) over 0.9 cm maximum radius spiral pattern. The slow raster frequency was the same frequency as the flipping of the beam helicity. Each of the rasters could independently be turned on or off and the raster size changed. The beam position was measured on an event-by-event basis using an array of secondary emission monitors [24] located upstream of the target.

At thermal equilibrium at 5 T and 1 K, the protons have a small polarization of 0.51% and the electrons have a large polarization of 99.8%. By applying a microwave radiation to the target material at a frequency near the electron spin-flip resonance frequency, the electron polarization is transferred to the proton. The protons have a slow relaxation time compared to the electrons and slowly the polarization of the protons builds up. The spin vector of the polarized protons is aligned parallel or anti-parallel to the field direction by changing the frequency of the microwaves and measurements were done at both microwave frequencies. For this data set, the target field was aligned at  $90^\circ$  to the beam direction with positive target polarization defined as the target field pointing toward beam left. The target polarization slowly decreased with exposure to the beam. When it became too small, the target was retracted from the beam to be annealed and repolarized.

The target polarization,  $P_T$ , was measured by the NMR technique. To extract absolute polarization, the NMR signal was calibrated by a known polarization at thermal equilibrium with no microwave radiation and no beam. Under these conditions, the proton polarization can be accurately calculated and used to determine the calibration constant,  $C_{TE}$ , of the NMR signal.  $C_{TE}$  was determined separately for the bottom and top target, since each target has an individual NMR setup. The normalization was taken from the weighted average of a series of thermal equilibrium (TE) measurements which gives a small statistical error on  $C_{TE}$ . To determine the systematic error on  $C_{TE}$ , three separate series of TE measurements were done for one target at different times and the standard deviation was found to be 2.9%. This was used as the relative systematic error on the target polarization for both targets.

The accelerator at Jefferson Lab produces highly polarized beam that can be simultaneously delivered to all three experimental halls. The polarized beam was produced by photo-emission from a semiconductor cathode using polarized laser light from a pulsed diode laser. Each hall had its own diode laser which produces a narrow pulse, but a small continuous noise was also present. This

produced a leakage current from the other hall's laser underneath the main beam pulse for that hall. The leakage current was measured in Hall C by an intrusive method. The rate in the HMS was measured with the Hall C laser turned on (normal conditions) and turned off (only leakage current). The ratio of the two rates is a measure of the leakage current. Throughout the experiment the leakage current was measured every 12 hours and on average the leakage current was found to be 2% of the total current. This is the leakage current from both Halls A and B.

The polarization of electrons produced at the cathode depends on the laser wavelength. At the time of this experiment, Hall A wanted high current and was not interested in polarized beam, while Halls B and C wanted low current and polarized beam. The wavelength of the laser chosen for the Hall A system produced a high current beam with  $\approx 35\%$  polarization which is about half the beam polarization for Hall C. A 2% leakage current from Hall A dilutes the Hall C beam polarization by about 1%. Since both Hall B and C were at the same laser wavelength, the beam polarization at the injector is the same for Halls B and C. This means that Hall B leakage current does not effect the polarization of beam to Hall C, but changes to the relative amount from Halls A and B to the total leakage current in Hall C does change the Hall C beam polarization. There was no measurement of the relative amount of leakage current from Halls A and B in the total measured leakage current. In addition to dilution from leakage current, the longitudinal beam polarization at the Hall C target depends on the energy per pass, the number of passes and the setting the spin rotator in the injector which was set to maximize the product of longitudinal beam polarization in Halls B and C. Therefore, to accurately know the beam polarization in Hall C, a measurement must be made near the Hall C target.

The beam polarization,  $P_B$ , was measured in Hall C using the Møller polarimeter [25]. Møller measurements were taken when the target was retracted from the beam for annealing. The Møller measurements were done at beam currents of 100 and 200 nA. The measurements were taken throughout the run period and are plotted in Fig. 2 as a function of run number. The average  $P_B$  was  $65.6 \pm 0.38\%$  and was used to determine the elastic asymmetry in Eq. 6. The beam polarization was assumed to be constant throughout the perpendicular target field running and no time dependent nor run-by-run adjustment to the beam polarization was done. The relative systematic error for the Møller measurement is 0.7%. The beam polarization could be different during the Møller measurements and the actual running due to changing leakage currents in Halls A and B. If the leakage current was mainly from Hall B then there would be no dependence of the Hall C beam polarization on leakage current. The worse case would be assuming that the leakage current is dominantly from Hall A. With that condition and assuming that leakage varies from 0% to 4% then

an estimate of the relative systematic error on the beam polarization from changes in the leakage current is 1%. Combining these errors in quadrature gives a relative systematic error of 1.3% on the beam polarization.

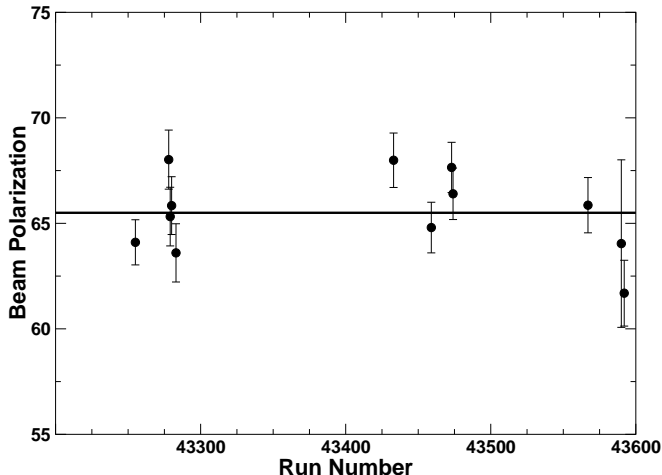


FIG. 2: Beam polarization,  $P_B$ , as a function of run number. The line is the weighted average of  $P_B$ .

When the target field is perpendicular to the beam direction, the incoming electrons are bent downward before the target by the magnetic field. Two chicane magnets before the target bend the incoming beam up so that, when combined with the target field, the beam is incident horizontally on the target. The electrons scattered toward the HMS are bent downward and have an average out-of-plane angle of  $3.4^\circ$ .

Normally, the position, angle and momentum of the scattered electron are determined by measuring HMS focal plane position and angles of the electron and then reconstructing the target quantities using an optics matrix. In addition, the HMS optics matrix takes into account the vertical position of the beam at the target. The calculation of momentum and out-of-plane angle are sensitive to the vertical position. The HMS optics matrix has been determined without the target field. The effect of the target field can be mimicked by using an effective vertical position at the target with the known HMS optics matrix in an iterative procedure. The reconstructed angles and momentum of the electron are determined using the known HMS optics matrix and an assumed effective vertical position at the target. The electron is tracked from the entrance of the HMS back through the target field to the center of the target using a tabulated map of the target field and the reconstructed electron momentum and angle. The difference is taken between this tracked vertical position at the target center and the vertical position of the beam measured by the SEM. If the difference is larger than 1 mm, then a new effective vertical position is assumed and the procedure is iterated until the difference between the tracked and measured vertical position is less than 1 mm.

To check the angle reconstruction, data were taken

with the sieve collimator which has a 9x9 grid of holes. The pattern of sieve holes were properly reconstructed by the algorithm described above. The momentum reconstruction was checked by looking at the reconstructed final state mass,  $W = \sqrt{M^2 + 2(E - E')M - Q^2}$ . The peak position of  $W$  was plotted as a function of different target variables. The  $W$  peak position had a slight dependence on the out-of-plane angle and no dependence on the other target variables. An azimuthal angle dependence was added to the map of the target field used in the calculation of the electron's track which changed the electron's reconstructed momentum and eliminated the dependence of  $W$  on the out-of-plane angle.

### III. EXPERIMENTAL RESULTS

From Ref. [26], the beam-target asymmetry,  $A_p$ , for elastic electron-proton scattering is related to the ratio of the proton's electric to magnetic form factors,  $r = G_E/G_M$ , by the formula:

$$A_p = \frac{-br \sin \theta^* \cos \phi^* - a \cos \theta^*}{r^2 + c} \quad (2)$$

in which  $\theta^*$  and  $\phi^*$  are the polar and azimuthal angles between the momentum-transfer vector,  $\vec{q}$ , and the proton's spin vector.  $a, b, c$  are kinematic factors:

$$a = 2\tau \tan \frac{\theta_e}{2} \sqrt{1 + \tau + (1 + \tau)^2 \tan^2 \frac{\theta_e}{2}} \quad (3)$$

$$b = 2 \tan \frac{\theta_e}{2} \sqrt{\tau(1 + \tau)} \quad (4)$$

$$c = \tau + 2\tau(1 + \tau) \tan^2 \frac{\theta_e}{2} \quad (5)$$

The measured asymmetry,  $A_m$ , is defined as  $(N^+ - N^-)/(N^+ + N^-)$  where  $N^+$  and  $N^-$  are the raw counts normalized for deadtime and charge for opposite beam helicities. The elastic asymmetry for the perpendicular target field is

$$A_p = \frac{A_m}{f P_B P_T} + N_c \quad (6)$$

where the measured asymmetry is normalized by  $P_T$ ,  $P_B$  and the dilution factor,  $f$ . The dilution factor is the ratio of the yield from scattering off free protons to that from the entire target.  $N_c$  is correction to the measured asymmetry which eliminates the contribution from quasi-elastic  $^{15}\text{N}$  scattering under the elastic peak.

In Fig. 3a, the yield,  $Y_{tot}$ , for scattering off the entire BOTTOM target is plotted versus  $W$ . The peak at  $W \approx 938$  MeV for elastic scattering off free protons is evident on top of the background from quasi-elastic scattering from other target material. The width of the elastic peak is  $\sigma = 14$  MeV and is determined by the resolution in the scattered electron's momentum and angle. The width is consistent with a combination of 1.5 mr resolution in  $\theta_e$

and  $1.5 \times 10^{-3}$  resolution in  $E'$ . These resolutions are about 50% larger than the typical resolutions found with no target field and smaller raster size.

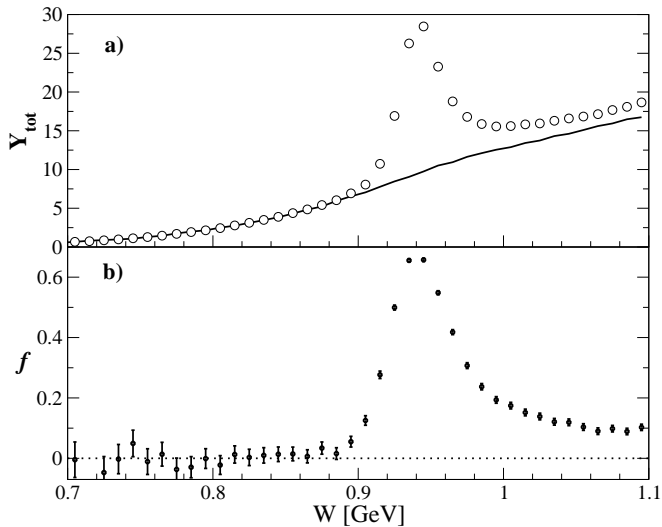


FIG. 3: a) The yield,  $Y_{tot}$ , for scattering from the entire BOTTOM target is plotted as open circles versus  $W$ . The error is smaller than the circle size. The solid line is  $Y_{back}$ , the  $^{12}\text{C}+\text{He}$  yield which has been normalized to  $Y_{tot}$  in the region of  $0.6 < W < 0.85$  GeV.

b) The dilution factor,  $f$ , for the BOTTOM target versus  $W$ . The dotted line indicates zero to guide the eye.

To determine the shape of the quasi-elastic background under the elastic peak, data were taken with a  $^{12}\text{C}$  disk (immersed in the liquid helium bath) of areal density comparable to the ammonia in the target. The solid line in Fig. 3a is the yield,  $Y_{back}$ , from the  $^{12}\text{C}+\text{He}$  data which has been normalized to the BOTTOM target yield in the region  $0.6 < W < 0.85$  GeV. The normalization factor was  $1.212 \pm 0.007$  for the BOTTOM target and  $1.235 \pm 0.007$  TOP target. One can see that the  $^{12}\text{C}+\text{He}$  matches the shape of  $^{15}\text{N}+\text{He}$  in the region  $0.6 < W < 0.85$  GeV. The assumption that the shape of the  $^{12}\text{C}+\text{He}$  is similar to the  $^{15}\text{NH}_3+\text{He}$  in the  $W$  region under the elastic peak was tested by a Monte Carlo simulation using realistic cross section models and including radiative corrections. The Monte Carlo predicts that normalization factor is 1.19 (1.22) for BOTTOM (TOP) target at  $W = 0.77$  GeV and has slight  $W$  dependence of 0.04 every  $\Delta W = 0.1$  GeV. The difference in normalization factor between the BOTTOM and TOP targets is caused by different packing fractions (the ratio of  $\text{NH}_3$  to helium in the target).

The dilution factor,  $f$ , is  $1 - Y_{back}/Y_{tot}$  and  $f$  for the BOTTOM target is plotted in Fig. 3b. In the calculation of the dilution factor, the  $W$  dependence of the normalization factor was not taken into account. For  $W < 0.85$  GeV,  $f$  is zero and flat indicating that the shape of the  $^{12}\text{C}+\text{He}$  data is well matched to the shape of the  $^{15}\text{N}+\text{He}$  background with a constant normalization at all  $W < 0.85$  GeV. Near  $W = 0.938$  GeV,  $f$  reaches a peak

of about 0.66 and drops off to near constant value of 0.10 for the  $W$  region of the elastic radiative tail up to pion production threshold ( $W = 1.075$  GeV). By combining the statistical error on the normalization factor and the error due to assuming a flat  $W$  dependence to the normalization factor, the relative systematic error of 1.1% on the dilution factor was calculated.

Typically, data taking was divided into runs of one hour duration and  $P_T$  changed during the run.  $P_T$  was continuously measured and recorded during the experiment every 20 seconds by an automated procedure. The average proton polarization for all runs was 66% (71%) when running with the BOTTOM (TOP) target. The charge-weighted average target polarization,  $P_T^{ave}$ , and  $A_m$  were measured for each run. In Fig. 4, the weighted average of  $A_m/P_T^{ave}$  for all runs is plotted as a function of  $W$  for BOTTOM and TOP targets.

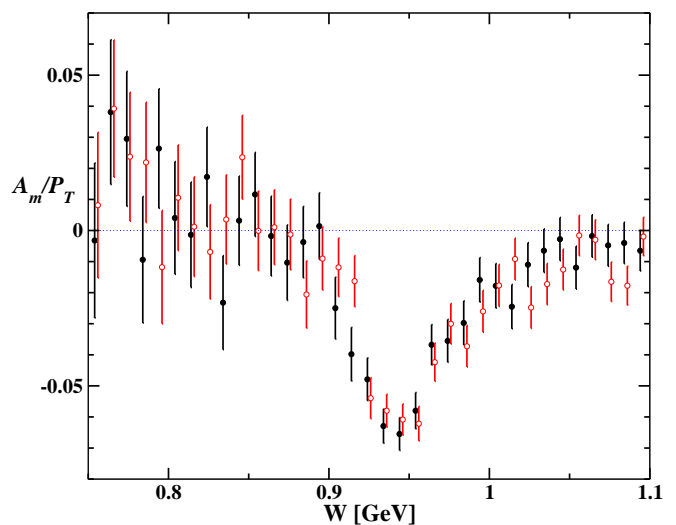


FIG. 4: (Color online) The asymmetry,  $A_m/P_T^{ave}$ , as a function of  $W$ . For the BOTTOM (TOP) target, the asymmetry is plotted as a solid (open) circle. Each data set is slightly shifted in  $W$  for clarity.

The protons in  $^{15}\text{N}$  are polarized and contribute to  $A_m$ . The contribution is characterized in terms of the correction term,  $N_c$ , in Eq. 6.  $N_c$  is equal to  $f_N/f \times P_N/P_T \times A_N$  in which  $f_N$ ,  $P_N$  and  $A_N$  are the dilution factor, polarization and asymmetry for the proton in  $^{15}\text{N}$ .  $A_N$  can be estimated from models [27]. From the angular momentum decomposition of the  $p_{1/2}$  level that is populated by the unpaired proton in the single particle shell model, one expects  $A_N = -A_p/3$ . The polarization of the proton in  $^{15}\text{N}$  relative to  $P_T$  has been measured in separate experiments [23, 28]. The data was fitted by the formula:

$$P_N = -0.01 \times (0.312 + 5.831|P_T| + 8.935|P_T|^2 + 8.685|P_T|^3)$$

For  $P_T = 71\%$  one gets  $P_N = -12\%$ . The dilution factor,  $f_N$ , is the ratio of the yield for scattering from the polarized proton in  $^{15}\text{N}$  to the yield from scattering from

the entire target.  $f_N$  is like  $f$  in that it varies with  $W$  and  $f_N = 0.03$  at  $W = 940$  MeV. The asymmetry is corrected for  $N_c$  at each  $W$  and, to give a flavor of the size of the correction,  $N_c = -0.0002$  at  $W = 940$  MeV which is a 0.2% correction to  $A_p$ .

$A_p$  is plotted as a function of  $W$  for both the BOTTOM and TOP targets in Fig. 5. For  $W < 0.9$  GeV,  $f$  is very small with relatively large error, so the error on  $A_p$  becomes larger than the scale of the y-axis. In the region  $0.9 < W < 1.0$  GeV,  $A_p$  is constant, and the error bars are small due to the large magnitudes of  $A_m/P_t$  and  $f$ . For  $W > 1.0$  GeV, in the region of the elastic radiative tail,  $A_p$  is still constant, but the error bars are larger. For the region  $0.9 < W < 1.0$  GeV, the average  $A_p$  is  $-0.1004 \pm 0.0042$  ( $-0.0994 \pm 0.0044$ ) for BOTTOM (TOP) target. Radiative corrections to  $A_p$  were calculated using the MASCARAD code of Ref. [29] and shift  $A_p$  by  $-0.0004$ . Including the radiative correction, the average  $A_p$  from both targets is  $-0.1003 \pm 0.0031$ .

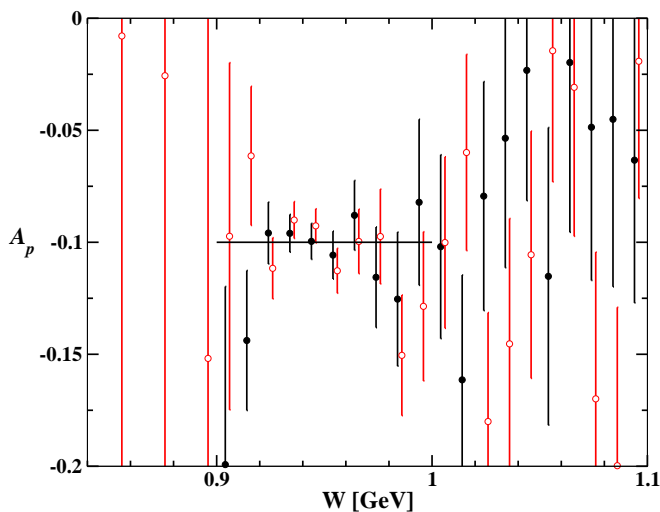


FIG. 5: (Color online) The asymmetry,  $A_p$ , as a function of  $W$ . For the BOTTOM (TOP) target, the asymmetry is plotted as a solid (open) circle. Each data set is slightly shifted in  $W$  for clarity. The solid line is the weighted average of  $A_p$  combining both targets.

Using Eq. 2,  $G_E/G_M$  can be determined directly from  $A_p$  using the formula:

$$\frac{G_E}{G_M} = -\frac{b}{2A_p} \sin \theta^* \cos \phi^* + \sqrt{\frac{b^2}{4A_p^2} \sin^2 \theta^* \cos^2 \phi^* - \frac{a}{A_p} \cos \theta^* - c} \quad (7)$$

in which  $a, b$  and  $c$  are the kinematic factors given in Eqns. 3-5. The average  $\theta_e$  is  $13.22^\circ$  and the average  $Q^2$  is  $1.509$   $(\text{GeV}/c)^2$ . The lab coordinate system is defined by the incoming and scattered electron's momentum vectors,  $k$  and  $k'$ , as positive  $z$ -direction along  $\hat{k}$ ,  $\hat{y} = \hat{k} \times \hat{k}'$  and  $\hat{x} = \hat{y} \times \hat{z}$  with  $+\phi$  rotation from  $+\hat{x}$  to  $+\hat{y}$ . Since

the scattered electron is bent downwards by the target's magnet field, the average azimuthal angle,  $\phi_e$ , is out-of-plane with a value of  $348.8^\circ$ . The  $\vec{q}$  points at the angles  $\theta_q = 50.43^\circ$  and  $\phi_q = 168.8^\circ$ . For Eq. 7, one needs the polar and azimuthal angles,  $\theta^*$  and  $\phi^*$ , between the  $\vec{q}$  and the proton's spin vector. Specifically, when the proton's spin vector is pointing at  $\theta_s = 90^\circ$  and  $\phi_s = 180^\circ$ ,  $\theta^*$  and  $\phi^*$  can be calculated by the formulas:

$$\theta^* = \arccos(\sin \theta_q \cos \phi_e)$$

$$\phi^* = 180 + \arctan \left[ \frac{\tan \phi_e}{-\cos \theta_q} \right]$$

For the present kinematics,  $\theta^* = 40.87^\circ$  and  $\phi^* = 197.26^\circ$ . With these kinematic factors and the radiatively corrected average  $A_p$ ,  $\mu G_E/G_M = 0.884 \pm 0.027$ . The solution to Eq. 2 for  $G_E/G_M$  is double-valued. The positive value of the square root was chosen, since the negative solution gives an unreasonable value of  $\mu G_E/G_M = -4.05$ . For this kinematic point, the systematic error on  $\Delta(G_E/G_M)/(G_E/G_M) = 0.97 \times \Delta A_p/A_p$ . The total relative systematic error on  $\mu G_E/G_M$  is 3.3%. A break down of the systematic errors is given in Table I. The beam and target polarization are the dominant contributions systematic contributions.

Variable	Error	$\Delta r/r$
$\theta_e$	0.5 mr	0.2%
$\theta^*$	0.1°	0.1%
$\phi^*$	1.0°	0.45%
$E$	0.003 GeV	0.005%
$E'$	0.005 GeV	0.01%
$f$	1.1%	1.1%
$P_T$	2.9%	2.8%
$P_B$	1.3%	1.3%
Total		3.3%

TABLE I: Relative systematic errors on  $r = G_E/G_M$ .

#### IV. CONCLUSION

In Fig. 6, the ratio  $\mu G_E/G_M$  from this experiment is compared to previous measurements. A recent global fit of  $G_E$  and  $G_M$  to the world cross section data has been done [3] and the result for  $\mu G_E/G_M$  is plotted by a dashed line in Fig. 6. The solid line is  $\mu G_E/G_M$  from a fit to all nucleon form factors by Lomon [30] which only uses proton  $G_E/G_M$  from the polarization transfer technique at large  $Q^2$ . The difference between the two curves is 12% at  $Q^2 = 1.509$   $(\text{GeV}/c)^2$ . The statistical error and systematic error for this measurement are comparable to previous  $\mu G_E/G_M$  values from cross-section and recoil polarization experiments. The data point is midway between the two curves so it is about  $2\sigma$  away from either curve. Unfortunately, the new measurement

does not help to determine whether the discrepancy between  $\mu G_E/G_M$  from the Rosenbluth technique and the polarization transfer technique is due to unknown systematic errors in either technique. At this  $Q^2$ , inclusion the Coulomb distortion effects [14] in the Rosenbluth technique would reduce  $\mu G_E/G_M$  by 0.05 which would make it overlap with the present data point and bring measurements from all three techniques into reasonable agreement.

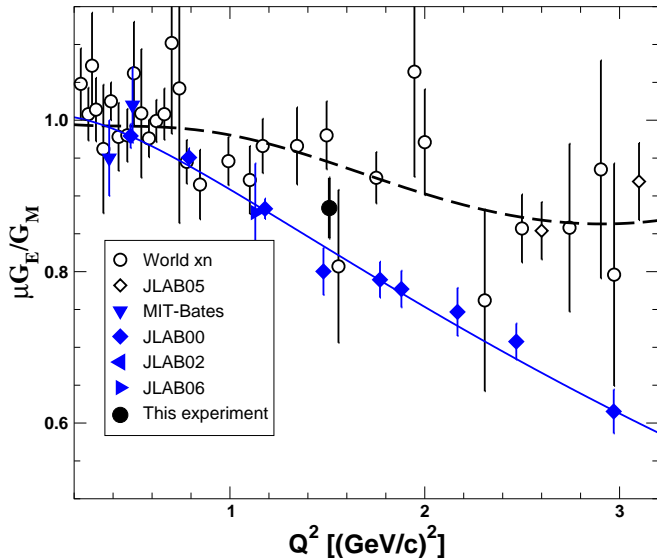


FIG. 6: (Color online) Ratio  $\mu G_E/G_M$  plotted as a function of  $Q^2$ . The ratio  $\mu G_E/G_M$  from this experiment is plotted as a filled circle with the error bar being the statistical and systematic error combined in quadrature. The solid line is a fit [30] to all form factor data, which only included proton  $G_E/G_M$  from Ref. [11] and [12] for large  $Q^2$ . Other symbols are same as in Fig. 1.

The inclusion of two-photon exchange mechanisms in the extraction of the Born cross section will reduce  $\mu G_E/G_M$  and bring it closer to  $\mu G_E/G_M$  determined by this measurement and previous measurements using the polarization transfer technique. A calculation [15] including all two-photon exchange mechanisms would reduce  $\mu G_E/G_M$  by about 0.08 compared to the dashed

line in Fig. 6. This beam-asymmetry measurement is at  $\epsilon = 0.963$  which minimizes the contribution from two-photon exchange mechanisms and, from Ref. [15],  $\mu G_E/G_M$  would be reduced by roughly a factor of 0.995 by accounting for the two-photon amplitude mechanisms.

This experiment is the first to measure  $G_E/G_M$  using beam-target asymmetry in elastic  $ep$  scattering. To definitively distinguish between experimental techniques at this  $Q^2$ , a beam-target asymmetry experiment needs to reduce both the statistical and systematic error. The systematic error which is hardest to reduce is the error on the target polarization. One approach would be to simultaneously measure the beam-target asymmetry at a given  $Q^2$  with two separate spectrometers which are at the same electron scattering angle but opposite sides of the beam. By taking the ratio of the two asymmetry measurements, the beam and target polarization will cancel and  $G_E/G_M$  can be extracted with no systematic from either polarization measurement. Another approach would be to measure at higher  $Q^2$  where the percentage difference between  $G_E/G_M$  extracted from the two experimental techniques is larger, since the systematic error on the beam and target polarization is independent of  $Q^2$ . To compensate for the falling cross-section, the experiment either has to run longer or use large acceptance detectors to keep the statistical error from growing too large. Dedicated experiments have been proposed [31, 32] at Jefferson Lab to measure  $G_E/G_M$  by beam-target asymmetries using both these experimental approaches.

### Acknowledgments

We would like to thank the Hall C technical staff and the accelerator operators for their efforts and dedication. This work was supported by Schweizerische Nationalfonds, the Department of Energy contract DE-FG02-96ER40950 and by the Institute of Nuclear and Particle Physics of the University of Virginia. The Southern Universities Research Association (SURA) operates the Thomas Jefferson National Accelerator Facility for the United States Department of Energy under contract DE-AC05-84ER40150.

- 
- [1] L. Andivahis *et al.*, Phys. Rev. D **50**, 5491 (1994).
  - [2] M. E. Christy *et al.* [E94110 Collaboration], Phys. Rev. C **70**, 015206 (2004).
  - [3] J. Arrington, Phys. Rev. C **69**, 022201 (R) (2004).
  - [4] I. A. Qattan *et al.*, Phys. Rev. Lett. **94**, 142301 (2005).
  - [5] A. I. Akhiezer and M. P. Rekalo, Sov. Phys. Dokl. **13**, 572 (1968) [Dokl. Akad. Nauk Ser. Fiz. **180**, 1081 (1968)].
  - [6] N. Dombey, Rev. of Mod. Phys. **41**, 236 (1969).
  - [7] A. I. Akhiezer and M. P. Rekalo, Sov. J. Part. Nucl. **4**, 277 (1974) [Fiz. Elem. Chast. Atom. Yadra **4**, 662 (1973)].
  - [8] M. J. Alguard *et al.*, Phys. Rev. Lett. **37**, 1258 (1976).
  - [9] C. E. Hyde-Wright and K. de Jager, Ann. Rev. Nucl. Part. Sci. **54**, 217 (2004).
  - [10] B. D. Milbrath *et al.* [Bates FPP collaboration], Phys. Rev. Lett. **80**, 452 (1998).
  - [11] V. Punjabi *et al.*, Phys. Rev. C **71**, 055202 (2005). M. K. Jones *et al.* [Jefferson Lab Hall A Collaboration], Phys. Rev. Lett. **84**, 1398 (2000).
  - [12] O. Gayou *et al.* [Jefferson Lab Hall A Collaboration], Phys. Rev. Lett. **88**, 092301 (2002).
  - [13] G. MacLachlan *et al.*, Nucl. Phys. A **764**, 261 (2006).
  - [14] J. Arrington and I. Sick, Phys. Rev. C **70**, 028203 (2004).



- [15] P. G. Blunden, W. Melnitchouk and J. A. Tjon, Phys. Rev. C **72**, 034612 (2005).
- [16] A. V. Afanasev, S. J. Brodsky, C. E. Carlson, Y. C. Chen and M. Vanderhaeghen, Phys. Rev. D **72**, 013008 (2005).
- [17] V. Tvaskis, J. Arrington, M. E. Christy, R. Ent, C. E. Keppel, Y. Liang and G. Vittorini, Phys. Rev. C **73**, 025206 (2006) [arXiv:nucl-ex/0511021].
- [18] Jefferson Lab Experiment E04-019, R. Gilman, L. Pentchev, C. F. Perdrisat and R. Suleiman, spokespersons.
- [19] Jefferson Lab Experiment E04-116, A. Afanasev, J. Arrington, W. Brooks, K. Joo and L. Weinstein, spokespersons.
- [20] J. Arrington, Phys. Rev. C **69**, 032201 (2004) [arXiv:nucl-ex/0311019].
- [21] J. Arrington *et al.*, proposal for an experiment at VEPP-3 (2004), [arXiv:nucl-ex/0408020].
- [22] Jefferson Lab Experiment E05-017, J. Arrington, spokesperson.
- [23] D. Crabb and D. Day, Nucl. Inst. Meth. **A356**, 9 (1995).
- [24] M. Steinacher and I. Sick, Nucl. Inst. Meth. **A455**, 759 (2000).
- [25] M. Hauger *et al.*, Nucl. Instrum. Meth. A **462**, 382 (2001)
- [26] T. W. Donnelly and A. S. Raskin, Annals Phys. **169**, 247 (1986).
- [27] O. A. Rondon, Phys. Rev. C **60**, 035201 (1999).
- [28] B. van den Brandt, *Proceedings of the 9th International Symposium on High energy Spin Physics, Bonn, 1990*, edited by K. H. Althoff, W. Meyer, E. Steffens and W. Thiel, (Springer-Verlag, Berlin, 1991), Vol. 2, p.289.
- [29] A. Afanasev, I. Akushevich and N. Merenkov, Phys. Rev. D **64**, 113009 (2001).
- [30] E. L. Lomon, Phys. Rev. C **66**, 045501 (2002).
- [31] G. Warren, Jefferson Lab Proposal P-01-105.
- [32] X. Zheng, J. Calarco and O. A. Rondon, Jefferson Lab Proposal P-04-014.